

SIZE AND STRUCTURE OF THE NARROW-LINE REGION OF QUASARS¹NICOLA BENNERT², HEINO FALCKE³, HARTMUT SCHULZ², ANDREW S. WILSON⁴, BEVERLEY J. WILLS⁵*Draft version October 22, 2018*

ABSTRACT

We have observed the narrow-line regions (NLRs) of the seven brightest radio-quiet PG (or BQS) quasars ($z < 0.5$) with the Wide Field and Planetary Camera 2 on board the Hubble Space Telescope (HST). Linear-ramp filters were used to image the [O III] $\lambda 5007$ line emission with $0''.0455$ – $0''.1$ pixel resolution. We find that the NLRs are very compact with typical extents of $2''$ – $4''$. Two quasars show compact filamentary structures similar to Seyfert NLRs. They may be related to radio outflows. Most interestingly, when including a sample of Seyfert galaxies observed with HST, we tentatively find that the size of the NLR is proportional to the square root of the [O III] luminosity. This is comparable to the scaling found for the size of the broad-line region with continuum luminosity, which has been interpreted in terms of a constant photoionization parameter. The relation determined here connects the NLR of radio-quiet quasars and Seyferts over three orders of magnitude in [O III] luminosity.

Subject headings: galaxies: active — galaxies: Seyfert — galaxies: structure — quasars: emission lines — quasars: general

1. INTRODUCTION

Quasars are active galactic nuclei (AGN) in which two different regions of ionized gas can be distinguished — the broad-line region (BLR) and the narrow-line region (NLR) which exhibit optical emission lines, kinematically broadened with typical widths of 10^3 – 4 km s^{−1} and 10^2 – 3 km s^{−1}, respectively. The optical spectra of quasars resemble those of the less luminous Seyfert galaxies, and it is presumed that most radio-quiet quasars are their more luminous counterparts. The most prominent optical emission lines of the NLR are [O III] $\lambda 5007$ (hereafter referred to simply as [O III]) and H α + [N II] $\lambda\lambda 6548, 6584$.

In the Unified Model of AGN, an optically thick obscuring dust torus is envisioned to encircle the accretion disk (Antonucci 1993), leading to a so-called “ionization cone” formed by anisotropic escape of ionizing photons (Schulz 1988; Pogge 1988, 1989; Storchi-Bergmann et al. 1992). Thus, the NLR is expected to show a specific morphology, which is suited for investigation with the high spatial resolution afforded by the Hubble Space Telescope (HST). Such investigations have been carried out for Seyfert galaxies, revealing highly elongated structures or ionization cones (Capetti et al. 1996; Falcke et al. 1998).

While the NLR in Seyferts is now relatively well studied, there are no comparable studies for the NLR in quasars. By observing quasars we can greatly extend the luminosity range to answer questions such as: Are quasars indeed just scaled-up versions of Seyferts? Does the size of the NLR scale with luminosity? Is this emission-line region possibly affected by radio jets shaping the interstellar medium, or is there a contribution from star formation?

We make a first step in this direction by presenting

an HST emission-line imaging survey of a complete sample of the seven brightest [in [O III], Boroson & Green (1992)] radio-quiet quasars from the BQS (Schmidt & Green 1983; Kellermann et al. 1989) with $z < 0.5$. The sample is given in Table 1. Here we present an investigation of the NLR structure as seen in the [O III] line and discuss the size of the NLR as a function of luminosity.

Luminosity distances for both Seyferts and quasars were calculated by using redshifts relative to the 3K background as derived with the velocity calculator provided by the NASA Extragalactic Database (NED). Throughout this paper we adopt a Hubble constant of $H_0 = 65$ km s^{−1} Mpc^{−1} and a homogeneous, isotropic, flat world model, which includes Einstein’s cosmological constant Λ in agreement with recent supernova measurements (Perlmutter et al. 1999): $\Sigma\Omega = 1$, $\Omega_{\text{matter}} = 0.35$, $\Omega_{\text{radiation}} = 0.05$, and $\Omega_{\Lambda} = 0.6$.

2. OBSERVATION, DATA REDUCTION, & ANALYSIS

2.1. HST Observations

All quasars in our sample were observed with the Wide Field and Planetary Camera 2 (WFPC2) on board HST between January and October 2000. Except for observations of the adjacent continua, we used the linear-ramp filters (LRFs). A description of properties and data reduction of LRF data is given in Falcke et al. (1998).

For our observations, the filters and central wavelengths were chosen to be centered on the redshifted [O III] emission lines. PG0026+129 was the only quasar that could be imaged with the Planetary Camera and its smaller pixel scale of $0''.0455$ pixel^{−1}. The other quasar images were taken with the Wide Field Camera ($0''.1$ pixel^{−1}). Several

¹ Based on observations with the NASA/ESA Hubble Space Telescope, obtained at the Space Telescope Science Institute, which is operated by AURA, Inc., under NASA contract NAS 5–26555

² Astronomisches Institut Ruhr-Universität Bochum, Universitätsstraße 150, D-44780 Bochum, Germany; email: nbennert@astro.ruhr-uni-bochum.de; email: hschulz@astro.ruhr-uni-bochum.de

³ Max-Planck-Institut für Radioastronomie, Auf dem Hügel 69, D-53121 Bonn, Germany; email: hfalcke@mpifr-bonn.mpg.de

⁴ Astronomy Department, University of Maryland, College Park, MD 20742–2421, USA; email: wilson@astro.umd.edu

⁵ Department of Astronomy and McDonald Observatory, University of Texas at Austin, Austin, TX 78712, USA; email: bev@pan.as.utexas.edu

short integrations of a bright star ($V = 11\text{--}16$) were taken in the LRF at the same position on the chips as the corresponding quasar, to determine the point-spread-function (PSF) for calibration purposes.

To subtract the underlying continuum, images of the adjacent continua were taken in narrow-band filters (F588N: $\delta\lambda = 49\text{\AA}$, F631N: $\delta\lambda = 30.9\text{\AA}$, and F673N: $\delta\lambda = 47.2\text{\AA}$), at the same chip position as the LRF images. All observations were split into several integrations to allow for cosmic-ray rejection with integration times chosen to avoid saturation at the position of the central point source.

2.2. Data Reduction & Analysis

All exposures were bias- and dark-subtracted and, except for the LRF images, flat-field corrected by WFPC2 pipeline processing at the Space Telescope Science Institute (STScI). For the LRFs, we used flat fields taken in nearby narrow-band filters. In all cases the different exposures were shifted (using linear interpolation as recommended for subsampled data) by aligning the central intensity peaks of the LRF, continuum, and PSF images, as determined from gaussian-profile fitting. The point-source calculator (as provided by STScI) was used for flux calibration. For subtraction of the continuum and especially the contribution from the unresolved continuum source at the center of the quasar, we used either the continuum images or the PSF star (see Table 1). In one case (PG1012+008), no continuum was detected on the continuum images, and a scaled PSF star was subtracted from the LRF image. The scaling was done such that, after subtraction, the central pixel had the same value as the average of the neighbouring pixels. This avoids “holes” in the center and may lead to an underestimate of the [O III] emission. We also had to scale the “continuum” image for PG1049-005 in the same way, as the image was, by accident, not taken in a continuum wavelength range but in the middle of the emission line of [O III] $\lambda 4959$. For PG0157+001 and PG0953+414 the continua were clearly extended compared with that of the PSF star, and the continuum images were used for subtraction. In the three remaining cases (PG0026+129, PG0052+251, and PG1307+085) the continua were not extended, compared with the PSF star, and we subtracted the PSF star, scaled to the flux seen in the continuum image, because of the higher signal-to-noise ratio of the star.

To check how much galaxy line emission or continuum we might be missing by using our short-exposure continuum (or scaled PSF) images, we used broad-band continuum images of the host galaxies of our quasars from Bahcall et al. (1997). The broad-band images were scaled to the appropriate filter width and exposure time of our LRF images and subtracted. We found the same [O III] flux at radii $> 2 - 10$ pixels, where the broad-band images were not overexposed, and concluded that, indeed, the host-galaxy continuum contribution to the LRF images was negligible outside the very nucleus. We also performed surface photometry of the continuum-subtracted LRF images and compared the resulting [O III] luminosities (Table 2) with the [O III] magnitudes determined by Boroson & Green (1992) with ground-based spectroscopy in a $6'' \times 1''.5$ extraction aperture. After correcting the luminosity distances for differences in the Hubble constant

(a 30% effect) and the world model ($\sim 3\%$), the difference between the HST imaging and ground-based spectroscopic data scatters within 0.25 mag, consistent with the expected spectrophotometric errors. The evidence suggests that we have not missed any significant extended flux, and that our continuum subtraction is correct.

3. RESULTS

3.1. Photometry & Structure

For each quasar we defined a radius of the NLR in our images at which a 3σ -level above background was reached in ring apertures. The surface brightness at that distance was typically 0.3% of central, thereby enclosing more than 98% of the detectable emission. The results of the photometry as well as these radii are given in Table 2. In all cases the NLR was largely concentrated within $2''\text{--}4''$.

Two quasars show compact filamentary structure as shown in Figure 1. Photometry of these features (PG0052+251: $\sim 1''.5$ to the south and $\sim 0''.8$ to the west of the nucleus; PG0157+001: $\sim 0''.4$ to the north and $\sim 1''$ to the west of the nucleus), was carried out separately (see Table 2). The feature in PG0052+251 can also be found in the broad-band images of Bahcall et al. (1997) as “knots” and in a radio map from Kukula et al. (1998) (classified as possible core-jet), whereas Miller et al. (1993) do not find a significant radio extension. The “linear” structure of PG0157+001 is coincident with radio features [Kukula et al. (1998) (classified as a double source with radio components on either side of the optical nucleus), Miller et al. (1993)]. A close association between the NLR emission-line morphology and that of the radio emission has already been found for Seyferts (Capetti et al. 1996; Falcke et al. 1998). PG1012+008 and PG0026+129 reveal some extended radio structure (Miller et al. 1993; Kukula et al. 1998), but we do not find extended emission-line features. Five out of the seven quasars are listed in Kukula et al. (1998) with maximum radio angular extents of $0''.24\text{--}2''$.

3.2. Size as a Function of Luminosity

An important question is how the NLR grows as one increases the luminosity of the central engine from Seyfert to quasar luminosities. For that reason we compared the sizes and luminosities of the NLR in our quasar sample with the NLR of a sample of Seyfert 2 galaxies that we have studied earlier. This sample was observed with HST in a very similar fashion, using LRFs and imaging the [O III] emission line (Falcke et al. 1998). In Figure 2 we plot the linear sizes versus the luminosities for the Seyferts and quasars.

The number of sources is of course very limited, but with the addition of the quasars we are probing three orders of magnitude in luminosity. The weighted linear least-square fit is (weight = σ^{-2} , σ = standard error in $\log R$; units of R and L are pc and erg/s, respectively):

$$\log(R_{\text{NLR}}) = (0.52 \pm 0.06) \log(L_{[\text{O III}]}) - (18.5 \pm 2.6) \quad (1)$$

with a correlation coefficient (cc) of 0.92 for 14 datapoints (dp). Hence, the size of the NLR seems to scale proportionally with the square root of the [O III] luminosity.

We note that for the quasars alone a similar relation is found, when plotting the NLR size versus the $H\beta$ luminosity (Figure 2, right). With $L_{H\beta}$ derived by multiplying our

$L_{[\text{O III}]}$ with the $\text{H}\beta/[\text{O III}]$ ratios from Boroson & Green (1992) (see Table 2) we obtain ($cc = 0.85$, 7 dp)

$$\log(R_{\text{NLR}}) = (0.67 \pm 0.15) \log(L_{\text{H}\beta}) - (25.5 \pm 6.3). \quad (2)$$

The average $[\text{O III}]/\text{H}\beta$ ratio of the Seyferts is 30 times larger than that of the quasars. Since the Seyferts are Type 2 objects, in the framework of the unified model, only a few percent of the total $\text{H}\beta$ is visible. Boroson & Green (1992) also found that $\sim 3\%$ of the total $\text{H}\beta$ flux is visible as the narrow line component. We have thus multiplied the inferred narrow line $\text{H}\beta$ luminosities of the Seyferts by a factor of 30 to estimate their total $\text{H}\beta$ luminosities, and found that the resulting R versus $L_{\text{H}\beta}$ relationship is consistent with an extrapolation to lower luminosity of the relationship found for the quasars. Including both Seyfert and quasar data into a weighted linear least-square fit we obtain ($cc = 0.91$, 14 dp)

$$\log(R_{\text{NLR}}) = (0.49 \pm 0.06) \log(L_{\text{H}\beta}) - (17.5 \pm 3.4). \quad (3)$$

4. DISCUSSION & CONCLUSIONS

We find that the NLRs of seven bright radio-quiet PG quasars are remarkably compact with typical extents of $2''$ – $4''$. Hence, detailed imaging of quasar NLRs requires sub-arcsecond resolution. Generally, the structure is relatively symmetric, in agreement with the unified scheme, that predicts a view into the ionization cones of these type 1 objects.

Two quasars exhibit compact filamentary structure like that seen for Seyferts. These structures may be related to radio outflows. This is reminiscent of the situation in many Seyfert galaxies, where radio outflows are morphologically related to the NLR. In three quasars the radio emission is approximately as compact as the NLR, and in all five cases that can be found in literature, the maximum angular extent is in agreement with our compact extents.

The NLR in quasars seems to be consistent with being a scaled-up version of the NLR in Seyferts. In fact, one of the Seyfert 2 galaxies, Mrk 34, has a similar radius and $[\text{O III}]$ luminosity to the quasars, and hence might be considered a “type 2 quasar”. In addition, the size of the NLR seems to scale roughly with the square root of the $[\text{O III}]$ luminosity when combining the quasar and Seyfert samples.

The latter result, however, has to be taken with some caution. For one, we have a very limited number of sources available. Especially for quasars, high resolution images of the NLR are extremely scarce, one essentially needs the resolution of HST plus the flexibility of the LRFs to image redshifted emission lines. Second, when comparing the Seyfert 2 and the quasar sample, one needs to consider that, according to the unified scheme, orientation effects might bias the type 2 sample towards somewhat larger sizes. Third, the individual scatter of NLR sizes is relatively large. Fourth, the “size” of the NLR is not a well defined quantity, being dependent on sensitivity and resolution. Nevertheless, given the large span in luminosities, none of the effects is likely to change the results significantly.

Seeking a clue to the origin of this relation, we consider a recombination line like $\text{H}\beta$, rather than $[\text{O III}]$, as a tracer of continuum luminosity. The ionization parameter is given by $U = Q/(4\pi c n_e R_u^2)$ (Q = rate of H-ionizing photons, R_u = distance between photoionizing source and emission-line clouds). Employing the relation $\omega Q = \alpha_B/(\alpha_{\text{H}\beta} h\nu_{\text{H}\beta}) = 3.9 \cdot 10^{12} L_{\text{H}\beta}$ (cgs units; ω is the covering factor and the recombination coefficients α_B and $\alpha_{\text{H}\beta}$ are taken from Osterbrock (1989) for $T = 2 \cdot 10^4 \text{K}$) yields a relation $R_u \propto L_{\text{H}\beta}^{0.5}$ for given U , n_e , and constant ω .

The slope in Figure 2 is close to the slope of 0.6 ± 0.1 given by Peterson (2001) for the relationship between BLR size (measured from reverberation mapping) and the continuum-luminosity (at 5100\AA). McLure & Jarvis (2002) find an even tighter correlation between BLR radius and 3000\AA luminosity, with both correlations being consistent with a relation of the form $R_{\text{BLR}} \propto L^{0.5}$.

To first order, BLRs and NLRs exhibit similar ionization parameters commonly explained by interaction of clouds with a quasar wind (Schiano 1986). More recently, Dopita et al. (2002) use radiation-pressure dominated photoionization models to explain a constant ionization parameter (in the range of $-2.5 \leq \log U \leq -2$). At the outskirts of a NLR, $n_e \sim 10^{2-3} \text{cm}^{-3}$, $U \sim 10^{-(2-3)}$, so that efficient $[\text{O III}]$ emission comes from regions with $U n_e \approx 1$, corresponding to an ionizing photon rate $Q/(4\pi R_u^2) = 3 \cdot 10^{10}$ photons/(s cm^2). Individual values of R_u derived with this scheme are slightly larger than the measured R , corresponding to covering fractions $\omega \leq 1$.

The same average $[\text{O III}]/\text{H}\beta$ ratio for Seyferts and quasars preserves the slope of the size- $[\text{O III}]$ relation for a size- $\text{H}\beta$ relation. This corroborates the explanation in terms of the ionization parameter and argues for photoionization as the main underlying process for producing narrow lines.

As pointed out by the referee, the relationship $L_{[\text{O III}]}$ (or $L_{\text{H}\beta}$) $\propto R_{\text{NLR}}^2$ corresponds to constant $[\text{O III}]$ (or $\text{H}\beta$) surface brightness. We are, however, not aware of any other physical, or instrumental, reason why this should be the case, since $[\text{O III}]$ is emitted by the whole *volume* filled with NLR clouds.

Clearly, more HST observations of quasars with lower $[\text{O III}]$ luminosity are needed to test the validity of the correlation. We expect fainter $[\text{O III}]$ quasars to have even smaller NLRs than the sources presented here and such a program will present an observational challenge for the years to come. Nevertheless, the available data provides the first direct evidence that quasar and Seyfert NLR are related and possibly evolve along a common luminosity-size track determined by photoionization.

N.B. thanks T. Jürges for computer support, C. Leipski for discussions, and R. Chini for financial support. This research was also supported by STScI through grant GO 8239 to the Universities of Maryland and Texas.

REFERENCES

- Antonucci, R.R.J. 1993, *ARA&A*, 31, 473
Bahcall, J.N., Kirhakos, S., Saxe, D.H., & Schneider, D.P. 1997, *ApJ* 479, 642
Bergvall, N., Johansson, L., & Olofsson, K. 1986, *A&A*, 166, 92
Boroson, T.A. & Green, R.F. 1992, *ApJS*, 80, 109
Capetti, A., Axon, D.J., Macchetto, F., Sparks, W.B., & Boksenberg, A. 1996, *ApJ*, 469, 554
Colina, L., Fricke, K.J., Kollatschny, W., & Perryman, M.A.C. 1987, *A&A*, 186, 39
Dopita, M.A., Goves, B.A., Sutherland, R.S., Binette, L., & Cecil, G. 2002, preprint (astro-ph/0203360)
Falcke, H., Wilson, A.S., & Simpson, C. 1998, *ApJ*, 502, 199
Cid Fernandes, R., Heckman, T., Schmitt, H., Delgado, R.M.G., Storchi-Bergmann, T. & 2001, *ApJ*, 558, 81C
Kaspi, S., Smith, P.S., Netzer, H., Maoz, D., Jannuzi, B.T., & Giveon, U. 2000, *ApJ*, 533, 631
Kellermann, K. I., Sramek, R., Schmidt, M., Shaffer, D. B., & Green, R. 1989, *AJ*, 98, 1195
Kukula, M.J., Dunlop, J.S., Hughes, D.H., & Rawlings, S. 1998, *MNRAS*, 297, 366K
McLure, R.J. & Jarvis, M.J. 2002, preprint (astro-ph/0204473)
Miller, P., Rawlings, S., & Saunders, R. 1993, *MNRAS*, 263, 425
Osterbrock, D.E.O. 1989, *Astrophysics of Gaseous Nebulae and Active Galactic Nuclei* (Mill Valley, CA: University Science Books)
Peterson, B.M. 2001, preprint (astro-ph/0109495)
Perlmutter, S., Aldering, G., Goldhaber, G. et al. 1999, *ApJ*, 517, 565
Pogge, R.W. 1988, *ApJ*, 328, 519
Pogge, R.W. 1989, *ApJ*, 345, 730
Schiano, A.V.R. 1986, *ApJ*, 302, 81
Schmidt, M. & Green, R.F. 1983, *ApJ*, 269, 352
Schulz, H. 1988, *A&A*, 203, 233
Storchi-Bergmann, T., Mulchaey, J.S., & Wilson, A.S. 1992, *ApJ*, 395, L73

TABLE 1
DETAILS OF OBSERVATION AND REDUCTION

Quasar (1)	α (2)	δ (3)	z (4)	Int. [O III] (5)	Int. Cont. (6)	Int. PSF Star (7)	Subtr. Method (8)
PG0026+129	00 29 13.71	+13 16 03.83	0.142	300 (8)	120 (2)	6 (2)	PSF star scaled to cont.
PG0052+251	00 54 52.13	+25 25 39.33	0.155	280 (5)	60 (4)	35 (4)	PSF star scaled to cont.
PG0157+001	01 59 50.21	+00 23 41.55	0.163	240 (6)	60 (4)	40 (4)	cont.
PG0953+414	09 56 52.35	+41 15 22.53	0.234	165 (8)	60 (4)	50 (4)	cont.
PG1012+008	10 14 58.10	+00 32 05.44	0.187	400 (4)	...	60 (3)	scaled PSF star
PG1049-005	10 51 51.46	-00 51 18.16	0.360	212.5 (8)	60 (4)	40 (4)	scaled cont.
PG1307+085	13 09 47.93	+08 19 49.62	0.155	250 (6)	60 (4)	35 (4)	PSF star scaled to cont.

Note. — Columns: (1) quasar; (2–3) right ascension (in units of hours, minutes, and seconds) and declination (degrees, arcminutes, and arcseconds) as provided by NED (J2000); (4) heliocentric redshift from NED; (5–7) mean of the integration time in s for the single image ([O III], continuum or PSF star) followed by, in brackets, the number of exposures which were combined; (8) subtraction method: scaled PSF star, continuum, scaled continuum or PSF star weighted by the flux in the continuum image

TABLE 2
EMISSION-LINE FLUX AND SIZE OF THE NLRs

Quasar (1)	Lum. Dist. (2)	Apert. (3)	Radius (4)	[O III] Flux (5)	[O III] Lum. (6)	H β Lum. (7)	Surf. Brightn. (8)
PG0026+129	708	0.86	2281 \pm 240	7	4.2 \pm 0.4	9.41 \pm 1.4	1.47
PG0052+251	780	1.39	3958 \pm 565	8.59	6.25 \pm 0.6	18.12 \pm 2.7	2.03
(feature)		0.6	1696 \pm 283	0.38	0.27 \pm 0.03	0.81 \pm 0.1	
PG0157+001	824	1.29	3832 \pm 590	5.67	4.61 \pm 0.5	7.74 \pm 1.2	2.43
(feature)		0.5	1474 \pm 295	0.4	0.32 \pm 0.03	0.54 \pm 0.1	
PG0953+414	1239	1.49	5884 \pm 785	3.14	5.76 \pm 0.6	49.9 \pm 7.5	1.05
PG1012+008	973	1.59	5319 \pm 665	5.01	5.67 \pm 0.6	20.35 \pm 3.1	1.54
PG1049-005	2011	1.99	10484 \pm 1048	5.64	27.28 \pm 2.7	52.57 \pm 7.9	0.53
PG1307+085	791	1.39	4002 \pm 572	6.96	5.21 \pm 0.5	20.83 \pm 3.1	1.35

Note. — Columns: (1) quasar; (2) luminosity distance in Mpc; (3) radius of the apertures in arcseconds; (4) radius of the NLR in pc; (5) [O III] λ 5007 fluxes, given in units of 10^{-14} erg s $^{-1}$ cm $^{-2}$. These fluxes were derived by summing the flux in the HST images inside the circular aperture with radius given in column (3); (6) [O III] λ 5007 luminosities in units of 10^{42} erg s $^{-1}$; (7) H β luminosities in units of 10^{42} erg s $^{-1}$; (8) surface brightness at the edge of the NLR in units of 10^{-17} erg s $^{-1}$ pixel $^{-1}$ (those of the Seyferts were at about the same value)

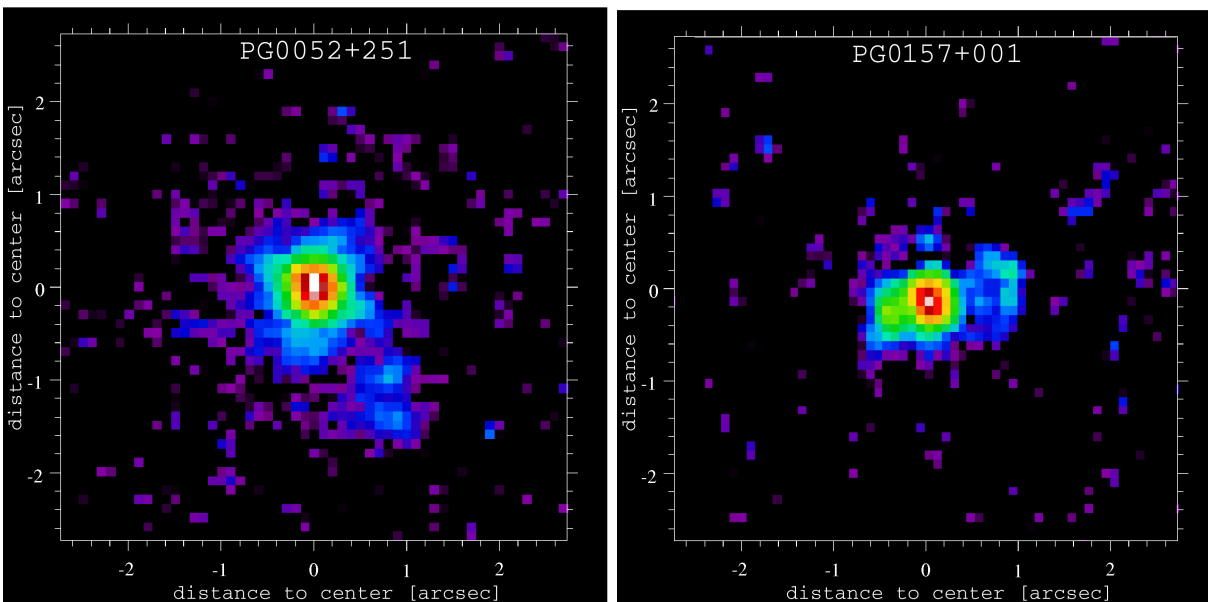


FIG. 1.— LRF images of PG0052+251 (left) and PG0157+001 (right) in [O III] λ 5007 in a logarithmic scale in false colours. North is up, east is to the left. The tick marks are chosen such that the central pixel is at 0 $^{\prime}$ 0; major tick marks are in distances of one arcsecond.

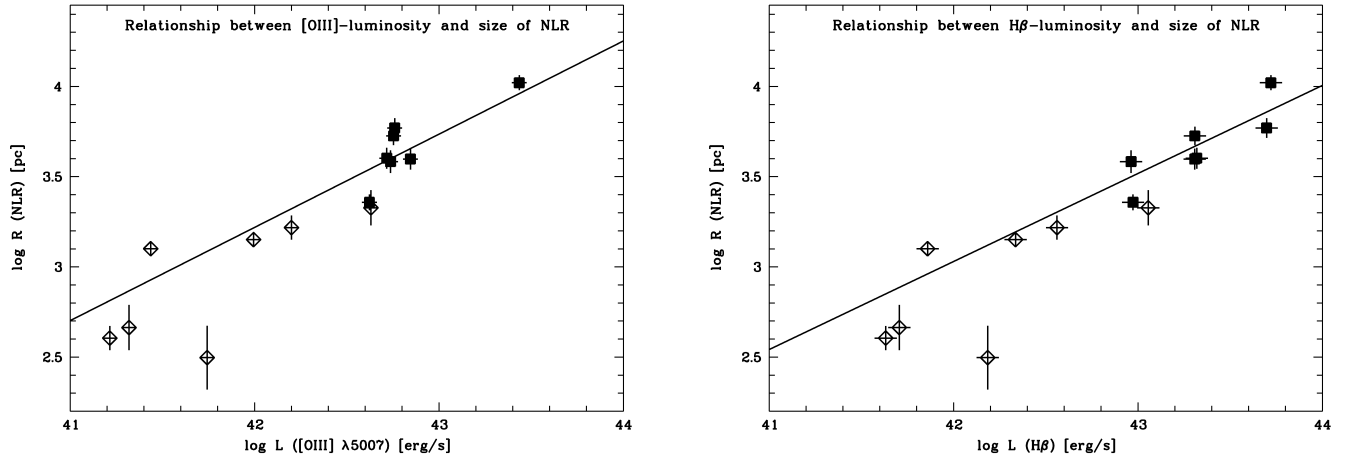


FIG. 2.— These panels show the radius of the NLR versus the emission-line luminosity in [O III] $\lambda 5007$ (left) and in $H\beta$ (right) on logarithmic scales. The open diamonds are Seyferts, the filled squares are PG quasars. The solid lines show weighted linear fits resulting in $R \propto L_{[\text{OIII}]}$ ^{0.52} (left hand panel) and $R \propto L_{H\beta}$ ^{0.49} (right). The error bars indicate the uncertainties in the fluxes from both the photometry and the placement of the apertures.